Support-Operators Method in the Identification of Permeability Tensor Orientation

Dmitriy B. Silin, Lawrence Berkeley Natl. Laboratory, and **Tad W. Patzek,** SPE, U. of California at Berkeley

Summary

The dependence of rock permeability on direction, or permeability anisotropy, is confirmed by numerous field examples. Therefore, the ability to carry out a numerical simulation of an anisotropic reservoir is very important. The support-operators method provides a conservative discretization scheme, allowing one to solve nonisotropic problems on a grid of practically arbitrary structure. Moreover, a discretization designed with the support-operators method provides a natural and convenient way of deriving and solving the adjoint system for evaluation of the gradient and second-order differential in inverse problems.

After a theoretical introduction into the support-operators method, we consider an illustrative parameter-identification problem. More specifically, we evaluate the orientation angle of a nonisotropic permeability tensor in a horizontal reservoir. We assume that the principal permeabilities near a cored or otherwise logged well are already known. To accomplish this task, we need pressure measurements in monitoring wells. We consider both rectangular and curvilinear grids. In either case, the orientation angle has been recovered with a high accuracy.

Introduction

Often, when modeling fluid flow in a porous rock, it is assumed that permeability of the rock is isotropic, at least horizontally (i.e., the permeability coefficient is the same regardless of the direction of pressure gradient). In other words, the direction of flow is aligned with the pressure gradient. This simplifying assumption cannot be accepted in every case. For example, the permeability of fissured rock is substantially dependent on microfractures; therefore, the dominating orientation of the fractures can make the direction of flow different from that of the pressure anti-gradient. Occurrences of anisotropy in oil reservoirs have been well documented (e.g., Refs. 1 and 2). Romm[3] provides several field examples in which measurements indicate the dependence of permeability on direction. Another field example with comprehensive well test data analysis is given in Ref. 4. The ratio of the maximum to the minimum permeability reported in the literature can be as large as 10^3. More references related to the studies of anisotropy of permeability in fractured reservoirs can be found in Ref. 5.

In general, anisotropy of a sedimentary formation results from the history of sedimentation. For example, an alluvial fan consists of stream-flow and debris-flow deposits and eolian sands. Strong horizontal anisotropy exists in the sediment transport direction and perpendicular to it. Thus, for realistic reservoir modeling, the ability to handle formation anisotropy is important. This requirement poses a challenge for a reservoir simulator developer, because standard numerical schemes usually assume either isotropic or diagonal tensors. In addition, if anisotropy is accompanied by heterogeneities, irregular curvilinear grids may be needed for appropriate discretization of the respective boundary-value problem. Methods for handling such situations are not broadly available in the petroleum literature. A split-tensor operator algorithm has been developed by Edwards.[6–8] Ref. 8 also includes a literature survey on methods of numerical treatment of problems with full permeability tensor.

The purpose of this article is to attract attention to a powerful method, different from the methods discussed in Ref. 8, that can be used to model flow in heterogeneous nonisotropic media on irregular grids. More specifically, we present an introduction to the support-operators method.

In this article, we emphasize the potential of the method per se, rather than analyze the performance of a specific reservoir or well pattern. Therefore, the presentation has a strong theoretical bias. Inasmuch as the focus of the method is on discretization of the Laplace operator (which equals the divergence of the flux in a combination with Darcy's law), we restrict ourselves to a steady-state problem, although a transient problem incorporating time derivatives can also be considered with appropriate modifications. To avoid cumbersome calculations that may hide the essence of the proposed approach, we consider a 2D problem only, but the method can be extended into 3D in a natural way.

Besides describing the discretization procedure, we show how the support operators can be used conveniently to solve inverse problems. We consider a simple synthetic example of an inverse problem, in which support operators facilitate numerical evaluation of the gradient of the data-fitting criterion through the adjoint system. Moreover, we extend the adjoint system analysis to calculate second-order differentials as well. The latter can be used to enhance the best-fit search by incorporating a Newton-type minimization method. Theoretically, it is known that under appropriate conditions, a Newton-type method provides a high-order and high-accuracy convergence to the minimum.

Calculation of first-order differential through adjoint system of differential equations provides clues into the sensitivity of the solution with respect to lumped or distributed parameters. An example of parameter of the first kind could be the total fluid content in the reservoir. The volumetric distribution of fluid saturation in the rock is an example of parameter of the second kind. The second differential is a much more complicated object; therefore, even such a powerful tool as adjoint system can provide only a directional differential. If the number of parameters is finite, then each second-order partial derivative has to be evaluated individually. Evaluation of second-order differential remains a complex task.

Clearly, an understanding of permeability anisotropy is important, for instance, when drilling new wells. There exist several techniques for analyzing permeability anisotropy. Some techniques rely on the modifications of injection-production models and respective well-test procedures for estimating permeability by matching well-test data. Although there is no consensus on which model is better,[9] the common idea is to match the data by an appropriate choice of the maximum and minimum permeability coefficient and appropriate orientation of the permeability tensor. In Ref. 5, the authors develop techniques to estimate the principal values of a nonisotropic permeability tensor

This paper (SPE 74709) was revised for publication from paper SPE 59372, first presented at the 2000 SPE/DOE Improved Oil Recovery Symposium, Tulsa, 3–5 April. Original manuscript received for review 25 April 2000. Revised manuscript received 25 May 2001. Manuscript peer approved 7 June 2001.

with single well-test data. In the example presented below, we assume that the principal permeabilities near a well are already known. Based on this information, we develop a method of estimating the angle of permeability-tensor orientation region surrounding the well. To accomplish this task, we need pressure measurements from nearby monitoring wells. As the result, we obtain an estimate of effective permeability tensor for the region where the measurements have been performed. Although the examples below are illustrative only, the method we develop can be applied in a much more general situation. The main components of the algorithm are the computation of the gradient and second differential of the minimized functional through the adjoint system of equations. An important property of the adjoint system is that it is linear with respect to the unknown function and that its structure is very similar to the structure of the forward problem. Often, the same code can be used for solving both of them. The support-operators method leads to a discretization that is convenient for deriving the discrete version of the adjoint system.

This paper is organized as follows. After formulating the underlying boundary-value problem, we discretize it using the method of support operators. Then we formulate an identification problem and obtain first and second differentials of the data-fitting criterion via first and second adjoint systems. We develop an algorithm of minimization of the functional and apply this algorithm on a rectangular and a curvilinear grid. To avoid unnecessarily overloading the presentation with algebra, the most intensive calculations are outlined in Appendices A through D.

Problem Statement

Consider a single-phase steady state pressure equation[10]:

$$\nabla \cdot \left(\vec{k} \nabla p \right) = -q \ ,.. \left(x, y \right) \in \Omega \ , \quad \ldots\ldots\ldots\ldots\ldots\ldots\ldots\ldots\ldots\ldots (1)$$

subject to the Dirichlet boundary condition

$$p\big|_{\Gamma} = p_0 \ . \quad \ldots\ldots\ldots\ldots\ldots\ldots\ldots\ldots\ldots\ldots\ldots\ldots\ldots\ldots\ldots\ldots (2)$$

Here, Ω = a two-dimensional domain and Γ = its boundary: $\Gamma = \partial\Omega$. At the boundary, the pressures are characterized by a known function p_0. The function q characterizes the rate of injection or production, depending on the type of the well. In this paper, we assume that the governing equations are already reduced to a dimensionless form.

The domain Ω is arbitrary with a reasonably regular boundary. We assume that permeability tensor $\vec{k}$ is symmetric and positive definite. To discretize the boundary-value problem in Eqs. 1 and 2, we make no specific assumption regarding the smoothness of $\vec{k}$. However, when we discuss the problem of evaluation of tensor orientation, it is assumed that $\vec{k}$ is constant over Ω and its principal values, k_1 and k_2, are already known. In that case, $\vec{k}$ can be represented as a rotation of the diagonal tensor $\begin{pmatrix} k_1 & 0 \\ 0 & k_2 \end{pmatrix}$ and, therefore, our goal is to estimate the rotation angle θ.

The structure of the grid is usually dictated by the heterogeneities of reservoir properties. The size of the grid is inferred from the accuracy considerations. In the context of this paper, we assume that the grid is already specified. Inasmuch as the grid can be of any shape and the permeability tensor may have nonzero off-diagonal elements, standard discretization schemes will not work. This is where the support-operators method enters the scene.

Support-Operators Method

The support-operators method was originally introduced in the early 1980s in the works by Shashkov, Samarski, and others (see Refs. 11 and 12). The main idea is that discretization should mimic the principal properties of the original boundary-value problem. Eq. 1 is derived from two physical principles: the mass balance and the momentum balance. The mass balance equation states that the divergence of the flux is equal to the density of sources, and, therefore, it is formulated in terms of divergence operator. The momentum balance equation relates the volumetric fluid flux u to the gradient of fluid pressure through Darcy's law: $u = -\vec{k}\nabla p$ (i.e., it is formulated in terms of the flux operator $\vec{k}\nabla p$). The divergence and gradient are two differential operators adjoint to each other through the Gauss-Ostrogradski divergence theorem (see Refs. 13 and 14). With a slight modification, the same conjugacy relationship holds true between the divergence and the flux.[11] Therefore, discretizations of divergence and flux that preserve the conservativeness of the boundary-value problem in Eqs. 1 and 2 also have to be adjoint to each other (i.e., should satisfy a discrete analog of the Gauss-Ostrogradski theorem). The support-operators method is based on these considerations. The resulting discrete version of Laplace operator on the left-hand side of Eq. 1 is a symmetric positive definite matrix. Moreover, the coordinate system invariance of this approach allows one to implement it on a practically arbitrary domain and grid. Many discretization techniques based on the finite-volumes method impose strict requirements on the orientation of gridblocks with respect to the flow direction.[15] It is very difficult to satisfy these grid-orientation requirements unless the solution is known beforehand.

Assume that domain Ω is discretized with a grid consisting of convex quadrilateral cells. Let us denote this grid by Ω_h, where subscript h stands for some characteristic size of a gridblock or a grid cell. We use quadrilateral gridblocks for simplicity only: in general, the grid may include cells of any shape. Denote by P a discrete array approximating the solution p of Eqs. 1 and 2. In each interior cell of grid Ω_h, P is equal to pressure p evaluated at the centroid of the cell. At the boundaries of Ω_h, the function p is evaluated in the middle of the boundary edge (edges, for the corner cells). We assume that the 2D grid Ω_h has $N_x \times N_y$ quadrilateral cells, enumerated by indices $i, j,\ 1 \le i \le N_x$, $1 \le j \le N_y$. The same indexing is applied to the array P in the interior cells: P_{ij} stands for the pressure evaluated at the centroid of cell (i, j). At the boundary, we shift the respective index by one half. For example, the values of P related to the left boundary have indices $P_{1/2\ j}$, $1 \le j \le N_y$ (see **Fig. 1**).

Following Refs. 11 and 12, we characterize the flux through each cell by four numbers f_{ij}^m, $m = 1, 2, 3, 4,$ equal to the normal components of the fluxes through the boundaries of the cell (i, j) (see **Fig. 2**). The positive orientation of the flow is north and east, so that fluxes $f_{ij}^{1,4}$ are evaluated along the inward normals, whereas fluxes $f_{ij}^{2,3}$ are evaluated along the outward normals. Denote by W the array of vectors characterizing the flux at the corners of the cells. In each cell (i, j), W_{ij}^m denotes the flux vector evaluated at the vertex m (see Fig. 2). Because, in general, the flux may be discontinuous at a given vertex, it may be evaluated differently in different cells. In other words, W may take up to four different values at each vertex. The relation between the arrays f and W is linear; therefore, it can be

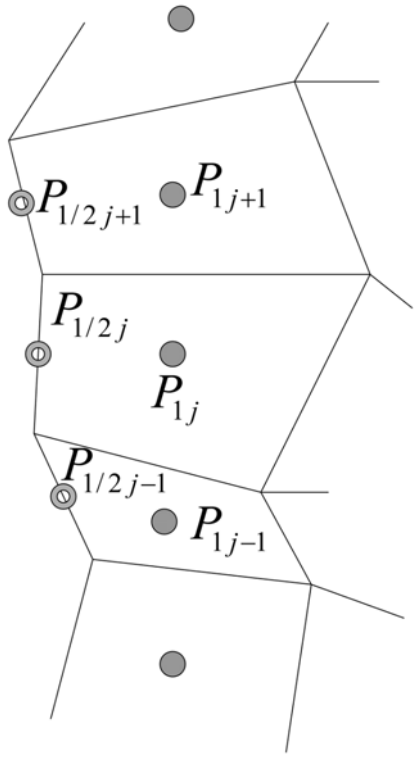

Fig. 1—Indexing of the interior and boundary cells.

characterized by a certain matrix $[\mathbf{\Phi}]$:

$$W = [\mathbf{\Phi}] f. \quad \text{.....(3)}$$

The elements of matrix $[\mathbf{\Phi}]$ can be found explicitly, and they depend only on the structure of grid Ω_h.

In Appendix A, we briefly outline the discretizations of divergence operator and the integral equality asserted by the Gauss-Ostrogradski theorem. The resulting formulae are given in Eqs. A-5 and A-18. In particular, Eq. A-18 implies that for an arbitrary array of fluxes *f* the following equality holds true:

$$\begin{aligned}&[\mathbf{\Phi}]^* [\mathbf{K^1}][\mathbf{B}][\mathbf{\Phi}][\mathbf{F}] P \cdot f \\ &= -[\mathbf{D}][\mathbf{\Lambda}] P \cdot f + [\mathbf{\Lambda_b}] P_b \cdot f_b\end{aligned} \quad \text{.....(4)}$$

The matrices in Eq. 4 are defined in Appendix A: $[\mathbf{K^1}]$ = a matrix derived from the inverse permeability tensor; $[\mathbf{B}]$ = the diagonal matrix of cubature (numerical integration in 2D) coefficients; $[\mathbf{F}]$ = the matrix of discretization of the flux operator; $[\mathbf{D}]$ = the discretization of the divergence operator; and $[\mathbf{\Lambda}]$ = a diagonal matrix whose elements are equal to the cell areas A_{ij}. The asterisk denotes matrix transposition. Matrix $[\mathbf{\Lambda_b}]$ is defined by the following equation:

$$\begin{aligned}[\mathbf{\Lambda_b}] P_b \cdot f_b = &\sum_{j=1}^{N_y} \left(P_{1/2\,j} f^1_{1\,j} l^1_{1\,j} + P_{N_x+1/2\,j} f^3_{N_x\,j} l^3_{N_x\,j} \right) \\ &+ \sum_{i=1}^{N_x} \left(P_{i\,1/2} f^4_{i\,1} l^4_{i\,1} + P_{i\,N_y+1/2} f^2_{i\,N_y} l^2_{i\,N_y} \right)\end{aligned}, \quad (5)$$

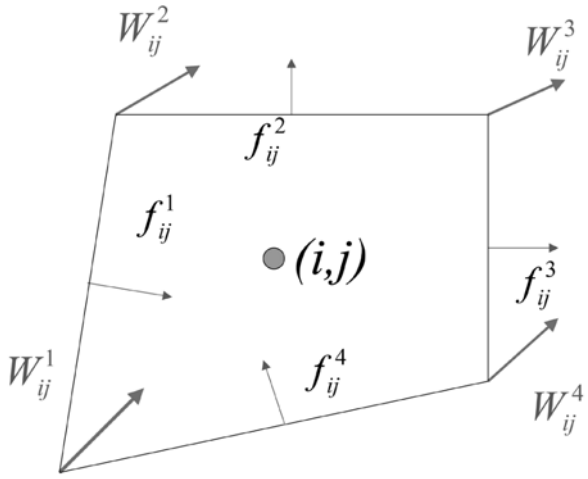

Fig. 2—Cell *(i,j)*: $f_{ij}^{1,2,3,4}$ are the normal components of the fluxes attached to the walls of the cell, while $w_{ij}^{1,2,3,4}$ are the fluxes at the corners of the cell.

cf. Eq. A-18. Here, l^m_{ij}, $m = 1,2,3,4$, are the lengths of the edges of cell (*i,j*) and subscript *b* stands for the boundary, so that Eq. 5 involves only the boundary values of *P* and *f*. It is important to remark that matrix $[\mathbf{K^1}][\mathbf{B}]$ is symmetric and positive-definite, and matrix $[\mathbf{\Lambda}]$ is diagonal with positive elements on the main diagonal.

Because we deal with a Dirichlet boundary-value problem, the boundary values of *P* are equal to the respective values of function p_0 (see Eq. 2). Because of the arbitrariness of *f*, Eq. 4 implies that

$$\begin{aligned}[\mathbf{F}] P = &-\left([\mathbf{\Phi}]^* [\mathbf{K^1}][\mathbf{B}][\mathbf{\Phi}] \right)^{-1} [\mathbf{D}][\mathbf{\Lambda}] P \\ &+ \left([\mathbf{\Phi}]^* [\mathbf{K^1}][\mathbf{B}][\mathbf{\Phi}] \right)^{-1} [\mathbf{\Lambda_b}] P_b\end{aligned} \quad \text{.....(6)}$$

Eq. 6 provides the discretization of the flux operator $\vec{k}\nabla p$ on grid Ω_h dual to the discretization of the divergence $[\mathbf{D}]$ in Eq. A-5. In general, the product $[\mathbf{\Phi}]^* [\mathbf{K^1}][\mathbf{B}][\mathbf{\Phi}]$ is a five-diagonal positive-definite matrix **(Fig. 3)**. For the case of rectangular grid and diagonal permeability tensor, it can be shown that matrix $[\mathbf{\Phi}]^* [\mathbf{K^1}][\mathbf{B}][\mathbf{\Phi}]$ is diagonal and $\left([\mathbf{\Phi}]^* [\mathbf{K^1}][\mathbf{B}][\mathbf{\Phi}] \right)^{-1} [\mathbf{D}]$ is a banded sparse matrix. Its structure is shown in **Fig. 4:** the dots denote nonzero elements, and the blank spaces correspond to zeros.

To construct a discretization of the boundary-value problem (Eqs. 1 and 2), we superpose the discretized divergence (Eq. A-5) and flux operator (Eq. 4):

$$\begin{aligned}&-[\mathbf{D}]\left([\mathbf{\Phi}]^* [\mathbf{K^1}][\mathbf{B}][\mathbf{\Phi}] \right)^{-1} [\mathbf{D}][\mathbf{\Lambda}] P = \\ &-Q + \left([\mathbf{\Phi}]^* [\mathbf{K^1}][\mathbf{B}][\mathbf{\Phi}] \right)^{-1} [\mathbf{\Lambda_b}] P_b\end{aligned} \quad \text{.....(7)}$$

Here, Q is the discretization of the source function q [i.e., Q_{ij} is equal to the average value of q in the cell (*i*, *j*)]. Applying the

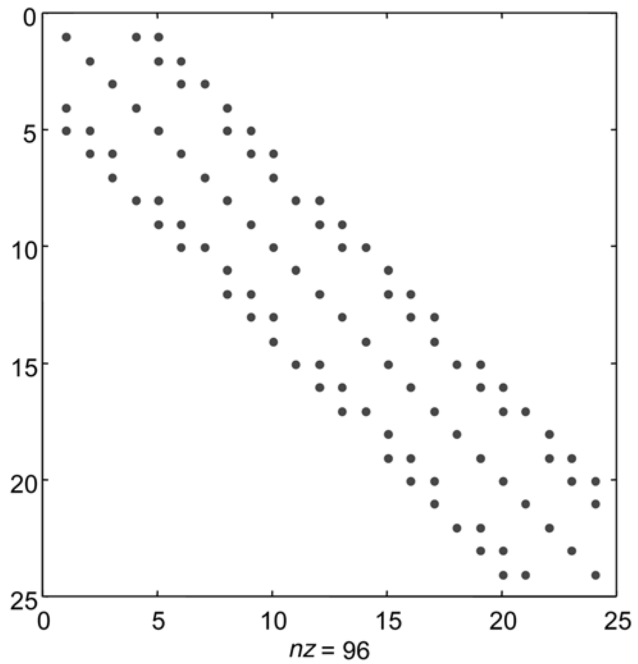

Fig. 3—The structure of the flux operator matrix on a rectangular grid. The *x* and *y* coordinates are the indices of the matrix elements. The elements that are nontrivial are denoted by dots; the zero elements are represented with spaces.

diagonal matrix $[\mathbf{\Lambda}]$ to both sides of Eq. 7, we obtain the following system of linear equations

$$[\mathbf{A}]P = B\,, \quad \text{.......}(8)$$

where

$$[\mathbf{A}] = [\mathbf{\Lambda}][\mathbf{D}]\left([\mathbf{\Phi}]^{*}\left[\mathbf{K}^{1}\right][\mathbf{B}][\mathbf{\Phi}]\right)^{-1}[\mathbf{D}][\mathbf{\Lambda}]\,, \quad \text{.......}(9)$$

and

$$B = [\mathbf{\Lambda}]Q - [\mathbf{\Lambda}]\left([\mathbf{\Phi}]^{*}\left[\mathbf{K}^{1}\right][\mathbf{B}][\mathbf{\Phi}]\right)^{-1}[\mathbf{\Lambda_b}]P_b\,. \quad \text{...}(10)$$

Clearly, it follows from Eq. 9 that matrix $[\mathbf{A}]$ is symmetric and positive definite, regardless of whether the grid is rectangular or not. It is possible to prove that if the grid is rectangular and the permeability tensor $\vec{\vec{k}}$ has zero off-diagonal elements, then matrix $[\mathbf{A}]$ has the same five-diagonal structure as the matrix produced by a standard finite difference scheme on a 5-point stencil[11,12] **(Fig. 5)**. In general, if either the grid is irregular or the off-diagonal elements of the permeability tensor are nonzero, both matrices $[\mathbf{F}]$ and $[\mathbf{A}]$ are full.

Estimation Problem

Assume that pressure measurements are available at certain points of domain Ω (e.g., through monitoring wells). Then our goal is to find a permeability tensor so that the numerical solution to the boundary-value problem in Eqs. 1 and 2 matches the measurements. Mathematically, the problem can be formulated in the following way: find the permeability tensor $\vec{\vec{k}}$ minimizing the fitting criterion

$$J\left[\vec{\vec{k}}\right] = \frac{1}{2}\int_{\Omega}\Xi(x,y)\left(p(x,y) - p_{*}(x,y)\right)^{2} d\Omega \quad \text{.....}(11)$$

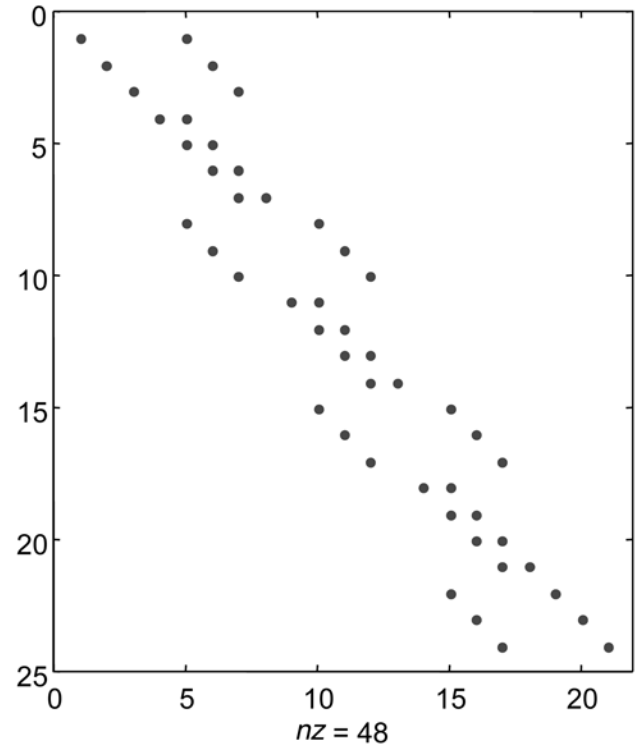

Fig. 4—The structure of discretized Laplace operator $\nabla\cdot\left(\vec{\vec{k}}\nabla p\right)$ on a rectangular grid. As in Fig. 3, the *x* and *y* coordinates are the indices of the matrix elements. The elements that are nontrivial are denoted by dots; the zero elements are represented with spaces.

subject to constraints (Eqs. 1 and 2). Here, $\Xi(x,y)$ is a nonnegative weight function, and $p_{*}(x,y)$ are the results of measurements. If the measurements are available only at one or several isolated locations

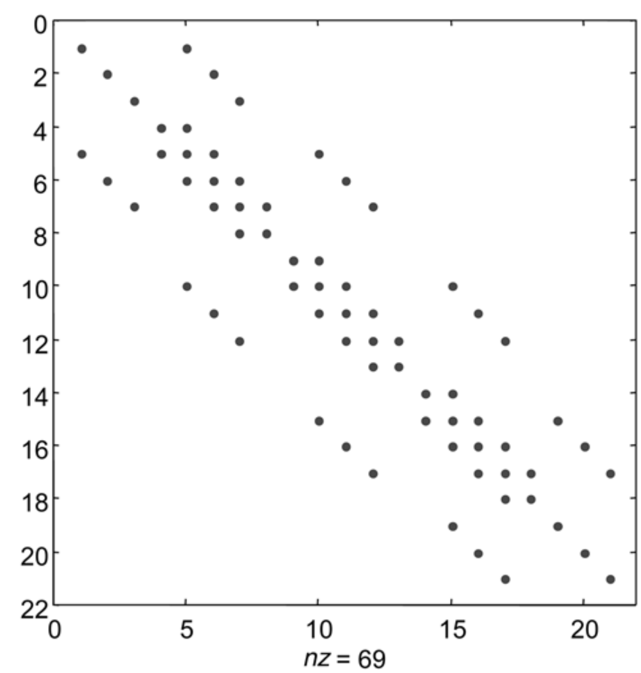

Fig. 5—The structure of the matrix $[\mathbf{\Phi}]^{*}\left[\mathbf{K}^{1}\right][\mathbf{B}][\mathbf{\Phi}]$ on an irregular grid.

locations with coordinates (x_i, y_i), i=1,2,...,N, then we put

$$\Xi(x,y)=\sum_{i=1}^{N}\delta(x-x_i,y-y_i), \quad \text{.....(12)}$$

where δ = Dirac's delta-function. In this case, the values of $p_*(x,y)$ outside the locations (x_i,y_i) do not matter for evaluating the functional in Eq. 11.

To minimize this functional numerically, we have to calculate its gradient (i.e., the linear part of its variation under a perturbation of the permeability tensor $\vec{\vec{k}} \to \vec{\vec{k}} + \delta\vec{\vec{k}}$). In Appendix B, we obtain that the gradient of the functional in Eq. 11 is equal to

$$\delta J = -\int_{\Omega} \nabla\psi \cdot \left(\delta\vec{\vec{k}}\nabla p\right) d\Omega, \quad \text{.....(13)}$$

where $\psi(x,y)$ = the solution of the adjoint boundary-value problem (Eqs. B-6 and B-7).

Eq. 13 provides exhaustive information about the sensitivity of the functional in Eq. 11 with respect to perturbations of the permeability tensor. Indeed, if, for instance, only the first element of $\vec{\vec{k}}$ is perturbed, then the respective sensitivity coefficient is obtained by substitution of $\delta\vec{\vec{k}} = \begin{pmatrix} \delta k_{11} & 0 \\ 0 & 0 \end{pmatrix}$ in Eq. 13. If tensor $\vec{\vec{k}}$ depends on one or more parameters, then to calculate the sensitivity of the functional in Eq. 11 with respect to these parameters, we need only to know the sensitivity of $\vec{\vec{k}}$ and substitute it in Eq. 13. Below, this argument is applied in the case where the permeability tensor depends only on the angle of orientation.

The formula for evaluation of the gradient, Eq. 13, is exact: the only sources of error are numerical solutions of the boundary-value problems and the numerical evaluation of the integral. If we tried to estimate the gradient by numerical differentiation, then we would inevitably introduce additional errors. Moreover, numerical differentiation approach may require solving the forward problem in Eqs. 1 and 2 many times, depending on the number of identification parameters. The adjoint boundary-value problem (Eqs. B-6 and B-7) is of the same type as the forward problem in Eqs. 1 and 2. Therefore, we can apply the support-operators method to discretize Eqs. B-6 and B-7 in the same way as it has been done for Eqs. 1 and 2.

Note that the gradient of the functional in Eq. 13 is expressed through ∇p and $\nabla\psi$. However, for computations we do not need to differentiate functions $p(x,y)$ and $\psi(x,y)$ numerically. Indeed, while constructing a discretization of the forward problem in Eqs. 1 and 2, we have derived matrix $[\mathbf{F}]$ approximating the flux operator $\vec{\vec{k}}\nabla p$. Therefore, we can put

$$\nabla p \approx \left[\mathbf{K^1}\right][\mathbf{\Phi}][\mathbf{F}]P \quad \text{and} \quad \nabla\psi \approx \left[\mathbf{K^1}\right][\mathbf{\Phi}][\mathbf{F}]\Psi. \quad \text{.....(14)}$$

Here Ψ is the discretization of adjoint variable ψ: Ψ_{ij} is equal to ψ evaluated at the centroid of cell (i,j).

As we have already mentioned earlier, our goal is to estimate the angle of orientation of the main axes of the permeability tensor $\vec{\vec{k}}$ if the eigenvalues k_1 and k_2 are known. Changing orientation of a symmetric positive definite tensor by an angle θ is equivalent to an orthogonal transformation of this tensor by the rotation matrix

$$[\mathbf{R}](\theta) = \begin{pmatrix} \cos\theta & -\sin\theta \\ \sin\theta & \cos\theta \end{pmatrix}. \quad \text{.....(15)}$$

Put

$$\vec{\vec{k}}(\theta) = [\mathbf{R}]^*(\theta)\vec{\vec{k}}_0[\mathbf{R}](\theta), \quad \text{.....(16)}$$

where $\vec{\vec{k}}_0 = \begin{pmatrix} k_1 & 0 \\ 0 & k_2 \end{pmatrix}$. Then,

$$\delta\vec{\vec{k}}(\theta) = \left[\frac{d}{d\theta}[\mathbf{R}]^*(\theta)\vec{\vec{k}}_0[\mathbf{R}](\theta) + [\mathbf{R}]^*(\theta)\vec{\vec{k}}_0\frac{d}{d\theta}[\mathbf{R}](\theta)\right]\delta\theta, \quad \text{.....(17)}$$

and from Eq. 13

$$\frac{dJ(\theta)}{d\theta} = -\int_{\Omega}\nabla\psi\cdot\left[\frac{d}{d\theta}[\mathbf{R}]^*(\theta)\vec{\vec{k}}_0[\mathbf{R}](\theta) + [\mathbf{R}]^*(\theta)\vec{\vec{k}}_0\frac{d}{d\theta}[\mathbf{R}](\theta)\right]\nabla p d\Omega. \quad \text{.....(18)}$$

In Appendix C, we derive the second order derivative of functional J with respect to θ:

$$\frac{d^2J(\theta)}{d\theta^2} = -\int_{\Omega}\nabla\psi\cdot\frac{d^2}{d\theta^2}\vec{\vec{k}}\nabla p d\Omega + \int_{\Omega}\nabla\psi_1\cdot\frac{d}{d\theta}\vec{\vec{k}}\nabla p d\Omega + \int_{\Omega}\nabla\psi_2\cdot\frac{d}{d\theta}\vec{\vec{k}}\nabla\psi d\Omega, \quad \text{.....(19)}$$

where the pair of functions ψ_1, ψ_2 is the solution to the system of two coupled boundary-value problems (Eqs. C-8 through C-11).

Solving the Estimation Problem

Clearly, the estimation problem formulated above cannot be solved analytically. The adjoint system (Eqs. B-6 and B-7) derived in Appendix B is a Dirichlet boundary-value problem for Poisson's equation of the same type as the forward problem in Eqs. 1 and 2. Therefore, the same discretization procedure based on the support-operators discussed above can be applied to solve Eqs. B-6 and B-7. Because matrix $[\mathbf{A}]$ in Eq. 8 is symmetric and positive definite, an iterative method such as conjugate gradients is very efficient. The problem of inversion of the aggregate matrix $\left([\mathbf{\Phi}]^*\left[\mathbf{K^1}\right][\mathbf{B}][\mathbf{\Phi}]\right)$ is not difficult because it is a five-diagonal symmetric positive definite matrix, and the method of conjugate gradients is very efficient in this case as well.

To evaluate the goodness of fit of the forward problem solution, we discretize the functional in Eq. 11. Because the numerically obtained solution P evaluates pressure p at the centroid of each cell, a natural discretization of the functional is provided by

$$J \approx \frac{1}{2}\sum_{i=1}^{N_x}\sum_{j=1}^{N_y}\Xi_{ij}\left(P_{ij}-P_{*ij}\right)^2 A_{ij}. \quad \text{.....(20)}$$

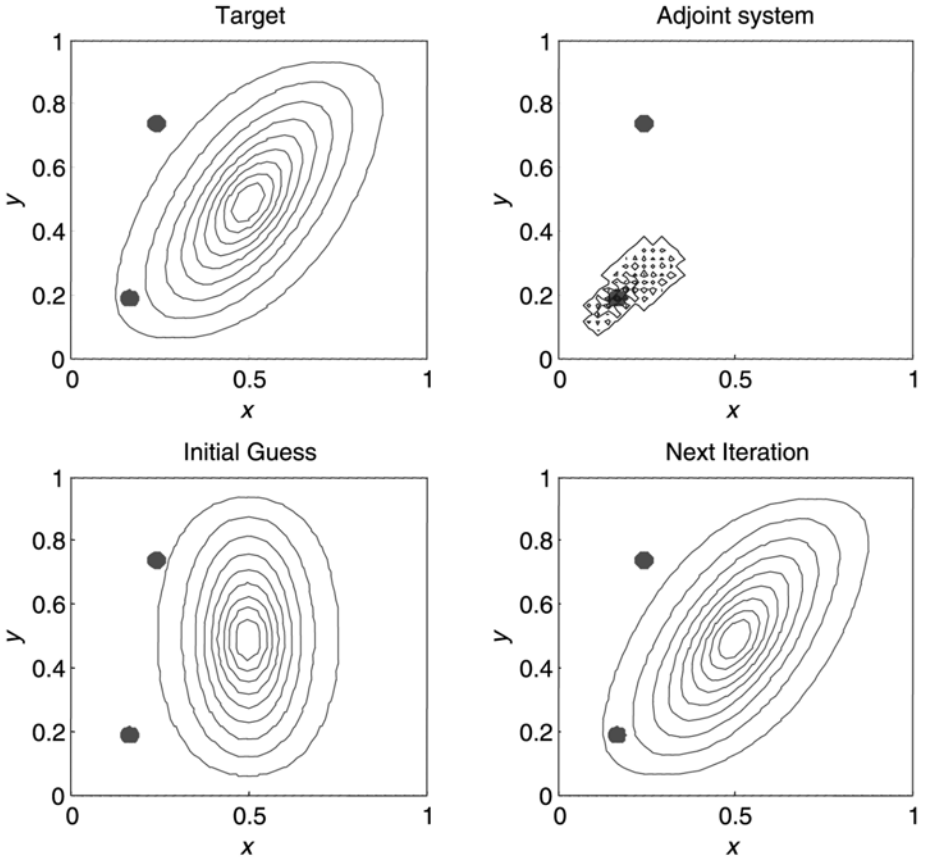

Fig. 6—Estimation of the permeability tensor orientation on a rectangular grid. The injector is in the center of the domain. All pressure plots are in dimensionless coordinates and normalized by the maximal values. The correct orientation is shown in the top left plot. The initial guess about the orientation angle is in the bottom left plot, and the final estimated orientation is in the right bottom plot. The two dots mark the locations of the monitoring wells. The accuracy of the rotation angle recovery is about 3×10^{-4} radians. The contour plot of solution to adjoint system looks irregular because this solution is fluctuating near zero in most parts of the domain, except for small neighborhoods of the locations of monitoring wells.

Here, Ξ_{ij} and P_{*ij} are the values of the weight function Ξ and the measured pressure p_* at the centroid of cell (i,j), and $|A_{ij}|$ = the area of the cell.

If we have only one observation point where the pressure is measured, the weight function Ξ is identically zero everywhere but in cell (i_0,j_0), where the measurements are available. Therefore, all the terms in Eq. 20, with the exception of the term with indices (i_0,j_0), vanish, and minimization of the functional reduces to minimization of a single term $\left(P_{i_0j_0}-P_{*i_0j_0}\right)^2$.

Evaluation of the gradient of the functional in Eq. 11 requires calculation of the gradients of the forward problem solution p and of the adjoint problem solution ψ. Computation of these gradients by numerical differentiation is problematic if we have a nonrectangular grid. However, the support-operators method furnishes the flux operator $[\mathbf{F}]$, so instead of explicit numerical differentiation, we apply Eq. 14. Thus, the discrete version of the gradient is given by

$$\frac{dJ}{d\theta}\approx[\mathbf{B}]\left[\mathbf{K}^{\mathbf{1}}\right][\mathbf{\Phi}][\mathbf{F}]\Psi\cdot\left[\tilde{\mathbf{K}}\right]\left[\mathbf{K}^{\mathbf{1}}\right][\mathbf{\Phi}][\mathbf{F}]P. \quad ...(21)$$

Here, $\left[\tilde{\mathbf{K}}\right]$ denotes the matrix generated by the derivative of the permeability tensor

$$\frac{d\vec{k}(\theta)}{d\theta}=\frac{d}{d\theta}[\mathbf{R}]^*(\theta)\vec{k}_0[\mathbf{R}](\theta) + [\mathbf{R}]^*(\theta)\vec{k}_0\frac{d}{d\theta}[\mathbf{R}](\theta). \quad .....(22)$$

Finally, the minimization algorithm can be organized in the following way. First, pick an initial guess θ_0. Then for each next iteration, θ_{n+1} is derived from θ_n using an iterative descent method:

$$\theta_{n+1}=\theta_n-\varepsilon_n[\mathbf{B}]\left[\mathbf{K}^{\mathbf{1}}\right][\mathbf{\Phi}][\mathbf{F}]\Psi\cdot\left[\tilde{\mathbf{K}}\right]\left[\mathbf{K}^{\mathbf{1}}\right][\mathbf{\Phi}][\mathbf{F}]P. \quad .....(23)$$

where P and Ψ are, respectively, the solutions of the forward and adjoint systems obtained at rotation angle θ_n. In the examples below, we determine the coefficient ε_n and the criterion for stopping iterations by Armijo's rule.[16] Eq. 23 is equivalent to Newton's method if

$$\varepsilon_n=\left(\frac{d^2J}{d\theta^2}\right)^{-1} \approx[\mathbf{B}]\left[\mathbf{K}^{\mathbf{1}}\right][\mathbf{\Phi}][\mathbf{F}]\Psi\cdot\left[\tilde{\tilde{\mathbf{K}}}\right]\left[\mathbf{K}^{\mathbf{1}}\right][\mathbf{\Phi}][\mathbf{F}]P$$

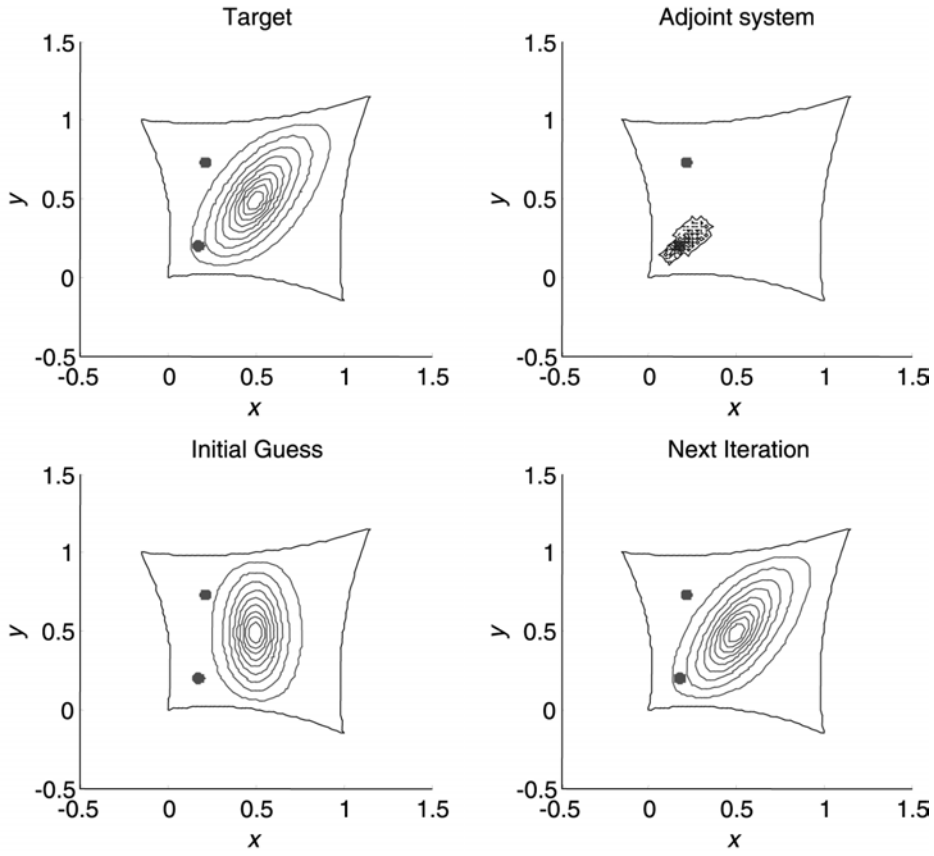

Fig. 7—Estimation of the permeability tensor orientation on a curvilinear grid with concave boundaries. The injector is in the center of the domain. All pressure plots are in dimensionless coordinates and normalized by the maximal values. The correct orientation is shown in the top left plot. The initial guess about the orientation angle is in the bottom left plot, and the final estimated orientation is in the right bottom plot. The dots mark the locations of the monitoring wells. The accuracy of the rotation angle recovery is about 5×10^{-4} radian. The contour plot of solution to adjoint system looks irregular because this solution is fluctuating near zero in most parts of the domain, except for small neighborhoods of the locations of monitoring wells.

$$+\left[\mathbf{B}\right]\left[\mathbf{K}^{\mathbf{1}}\right]\left[\mathbf{\Phi}\right]\left[\mathbf{F}\right]\Psi_1\cdot\left[\tilde{\mathbf{K}}\right]\left[\mathbf{K}^{\mathbf{1}}\right]\left[\mathbf{\Phi}\right]\left[\mathbf{F}\right]P$$

$$+\left[\mathbf{B}\right]\left[\mathbf{K}^{\mathbf{1}}\right]\left[\mathbf{\Phi}\right]\left[\mathbf{F}\right]\Psi_2\cdot\left[\tilde{\mathbf{K}}\right]\left[\mathbf{K}^{\mathbf{1}}\right]\left[\mathbf{\Phi}\right]\left[\mathbf{F}\right]\Psi, \quad .....(24)$$

where $\left[\tilde{\tilde{\mathbf{K}}}\right]$ denotes the matrix generated by the second derivative of the permeability tensor and Ψ_1 and Ψ_2 are the solutions of discretized adjoint Eqs. C-8 and C-11 at $\theta=\theta_n$.

In the approach we have been developing so far, the adjoint system and the gradient are obtained first, and both the forward and the adjoint problems are discretized simultaneously. An alternative approach is to begin with discretization of the forward problem and the functional, and then to obtain the adjoint system and the gradient for the discretized forward problem. In such a way, we do not derive the differential adjoint equation, but immediately obtain a discrete system. In Appendix D, we derive the relevant equations. Normally, derivation of the adjoint system to the already discretized equations leads to severe difficulties because calculations involve multiple indices and are quite cumbersome. The framework of the support-operators method simplifies these calculations significantly.

As in Appendix C, we could derive the discrete second adjoint equations and obtain the second derivative of the functional in Eq. 20. However, we do not present these results here.

There is no obvious preference of either method: the adjoint system first and discretization after that, or vice versa. Error in estimating the gradient by the first approach originates from the numerical solution of the forward and adjoint boundary-value problems and from truncation errors in evaluating the gradient (see Eq. 21). The second approach provides the gradient of the discrete functional only subject to round-off computational errors. However, from the very beginning, we replace the original problem with its discrete approximation. In particular, this results in more cumbersome calculations. In test examples, we observed no dramatic difference in the results produced by the two methods.

Example. To illustrate the method developed above, let us consider the following example. We generate the target solution by solving a forward problem (Eqs. 1 and 2) with zero boundary condition and permeability tensor $\vec{\vec{k}}_*=\begin{pmatrix}7.75 & 3.90\\ 3.90 & 3.25\end{pmatrix}$ that corresponds to a rotation of the diagonal tensor $\begin{pmatrix}10 & 0\\ 0 & 1\end{pmatrix}$ by $\frac{\pi}{6}$. We take the source function f and the weight function w as approximations to Dirac's delta function. Assuming various initial guesses of the rotation angle θ, we apply the gradient descent method with Armijo's rule of selecting the gradient step ε and the criterion for stopping iterations. The algorithm is implemented in Matlab, so we do not need to bother about inverting matrices or solving systems of linear equations. On a rectangular grid, the initial value of the functional 1.9 has been reduced to 3.6e-7, and

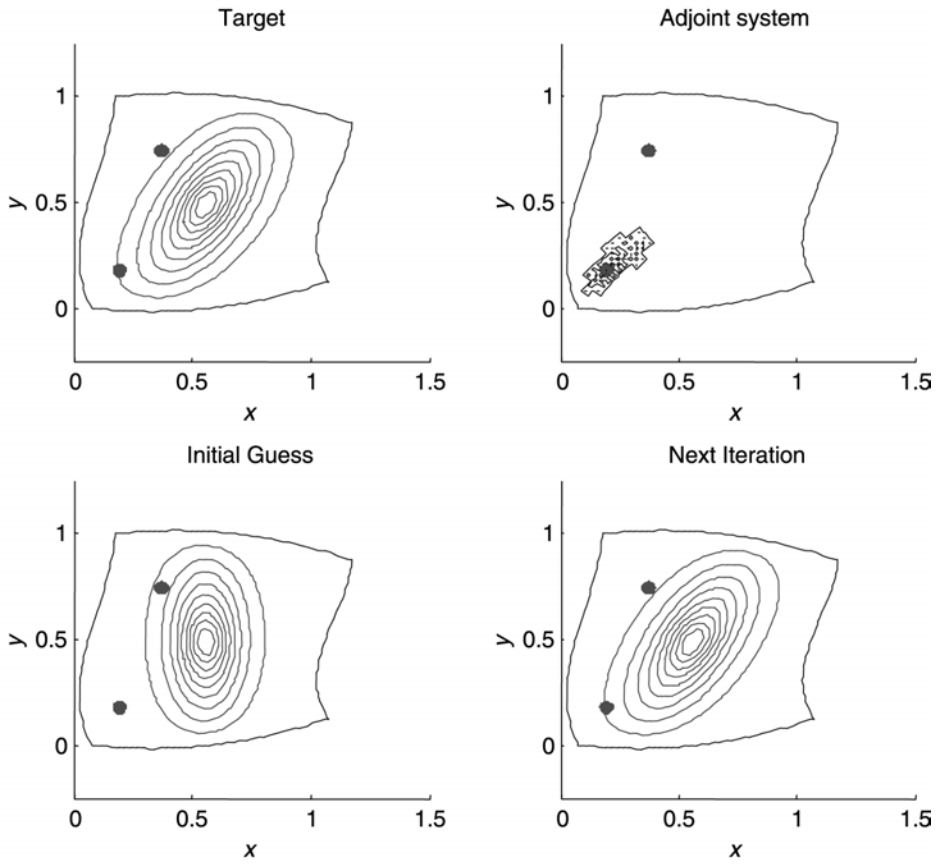

Fig. 8—Estimation of permeability tensor on a curvilinear grid 2 with both convex and concave boundaries. The injector is in the center of the domain. All pressure plots are in dimensionless coordinates and normalized by the maximal values. The correct orientation is shown in the top left plot. The initial guess about the orientation angle is in the bottom left plot and the final estimated orientation is in the right bottom plot. The dots mark the locations of the monitoring wells. The accuracy of the rotation angle recovery is about 5×10^{-4} radian. The contour plot of solution to adjoint system looks irregular because this solution is fluctuating near zero in most parts of the domain, except for small neighborhoods of the locations of monitoring wells.

the angle of rotation has been found with absolute error of 1.3e-4. Tensor $\vec{\vec{k}}_*$ has been identified with absolute error of 1e-3. The results of application of the algorithm on two curvilinear grids are presented in **Figs. 6 through 8** and **Table 1.** The number of iterations and the elapsed time of computations depend on the grid. Curvilinear grid takes more time because the flux matrix is full. The number of iterations of descent method depends on how "lucky" we are with the initial guess. Clearly, the functional in Eq. 11 and its discrete approximation in Eq. 20 are periodic functions of θ, the minima (best fit) of which are alternating with maxima (worst fit). If the initial guess is close to the maximum of Eq. 11, then the first iterations move slowly toward the minimum, because the gradient is close to zero. Then the iterations accelerate and we observe linear convergence to the minimum. In all the examples presented here, the initial guess was "bad enough": $\theta_0 = -\frac{\pi}{6}$. In Figs. 6 through 8, the top left plot is the graph of the target solution. The left bottom plot is the graph of the initial guess. In the right top plot, we graph the solution of the adjoint boundary-value problem. As we can observe, $\psi(x,y)$ is almost equal to zero everywhere outside of a small neighborhood of the point where the target solution is evaluated and in which the weight function Ξ is not equal to zero. The location of the domain in which the adjoint variable is nonzero shows that the sensitivity of the functional in Eq. 20 with respect to the measurements at the well located near the left bottom corner of the domain is much higher than with respect to the measurements at the other well.

The right bottom plot is the graph of the solution obtained forthe recovered value of θ. Close similarity to the plot of the target function needs no comment.

TABLE 1—RESULTS OF COMPUTATIONS

Figure	Initial Value of the Functional	Final Value of the Functional	Absolute Error of Angle Estimation
Fig. 8	1.93	3.6e-007	1.3e-004
Fig. 9	2.35	5.0e-006	4.5e-004
Fig. 10	1.51	3.0e-007	1.3e-004

Conclusions

1. A procedure of discretizating Laplace operator based on support operators is described. This procedure can be applied in numerical fluid-flow simulations on an irregular grid with a fully anisotropic permeability tensor.
2. The procedure can be equally well applied to discretize the flow equations in an arbitrary coordinate system in a highly heterogeneous medium.
3. An illustrative problem of estimation of the orientation angle of an anisotropic permeability tensor has been formulated.
4. In this problem, the first and second differentials of a quadratic data-fitting criterion have been obtained through the adjoint-system approach.
5. Both the forward and adjoint problems have similar structures. The support-operators method provides a natural and convenient framework for discretization of both forward and adjoint problems. The adjoint systems have been derived in continuous and discretized forms.
6. The numerical method for solving the forward boundary-value problem can be applied to solving the adjoint problems of first and second order. Therefore, common subroutines can be used.

7. A minimization algorithm based on the formulae for the gradient and discretization by the support-operators method has been developed. The algorithm has been verified on several synthetic examples involving computations on rectangular and curvilinear grids. The algorithm demonstrated good convergence to the minimum, and recovery of the searched angle of orientation of the permeability tensor is estimated with good precision. The algorithm has been implemented in Matlab.

Nomenclature

$[\mathbf{A}]$ = matrix of coefficients of discretized equations

A_{ij} = volume (here area) of cell (i,j)

B = right side of the system of discretized equations

$[\mathbf{B}]$ = matrix of cubature coefficients

$[\mathbf{D}]$ = matrix of discretized divergence operator

f, f_{ij}^m = discretized normal component of a dummy vector field

$[\mathbf{F}]$ = matrix of discretized flux operator

i, j, m = dummy indices

J = fitting criterion

$\vec{\vec{k}}$ = permeability tensor

$[\mathbf{K}^1]$ = matrix derived from the inverse permeability tensor

$[\tilde{\mathbf{K}}], [\tilde{\tilde{\mathbf{K}}}]$ = matrices generated by first and second derivative of the permeability tensor

l_{ij}^m = areas (here lengths) of the side faces of the grid cell (i, j)

Nx, Ny = dimensions of the grid

q, Q, Q_{ij} = density of sources, continuous and discretized

$[\mathbf{R}]$ = matrix of rotation

p, P, P_{ij} = pressure, continuous and discretized

p, P_*, P_{*ij} = measured pressure, continuous and discretized

u, U, U_{ij} = volumetric flux, continuous and discretized

w, W, W_{ij}^m = dummy vector field, continuous and discretized

x, y = cartesian coordinates

z, Z_{ij}^m = scalar product of two vector fields, continuous and discretized

β_{ij}^m = cubature coefficients

Γ = boundary of the domain on which the equations are solved

ε_n = step size in gradient descent method

θ = angle of orientation of the permeability tensor

$[\mathbf{\Lambda}]$ = diagonal matrix with the volumes of the grid cells on the main diagonal

Ξ = weight function

$[\mathbf{\Phi}]$ = matrix of transformation of a discretized vector field into an array of normal fluxes

ψ, ψ_1, ψ_2 = solutions of first and second adjoint problems

Ψ, Ψ_1, Ψ_2 = discretized solutions of first and second adjoint problems

Ω, Ω_h = domain and discretized domain on which the equations are being solved

Acknowledgments

This work was supported in part by a member of the U. of California Oil® Consortium, Chevron U.S.A. Partial support was also provided by the Assistant Secretary for Fossil Energy, Office of Gas and Petroleum Technology, under contract No. DE-ACO3-76FS00098 to the Lawrence Berkeley Natl. Laboratory of the U. of California.

References

1. Elkins, L.F.: "Reservoir Performance and Well Spacing—Silica Arbuckle Pool," *Drill. and Prod. Prac., API* (1946) 109.
2. Elkins, L.F. and Skov, A.M.: "Determination of Fracture Orientation From Pressure Interference," *JPT* (December 1960) 301.
3. Romm, E.S.: *Permeability Properties of Fissured Rock (in Russian),* Nedra Publishers, Moscow (1966).
4. Ramey, H.J.: "Interference Analysis for Anisotropic Formations–A Case History," *JPT* (October 1975) 1290.
5. Guo, B., Schechter, D.S., and Banik, A.: "Use of Single-Well Test Data for Estimating Permeability Anisotropy of the Naturally Fractured Spraberry Trend Area Reservoirs," paper SPE 39807 presented at the 1998 SPE Permian Basin Oil and Gas Recovery Conference, Midland, Texas, 1–4 October.
6. Edwards, M.G. and Rogers, C.F.: "Finite Volume Discretization With Imposed Flux Continuity for the General Tensor Pressure Equation," *Computational Geosciences* (1998) **2,** 259.
7. Edwards, M.G.: "Split Elliptic Tensor Operators for Reservoir Simulation," *Proc.,* ICFD Conference on Numerical Methods for Fluid Dynamics, Oxford U., Oxford, U.K. (1998).
8. Edwards, M.G.: "Simulation With a Full-Tensor Coefficient Velocity Field Recovered From a Diagonal-Tensor Solution," *SPEJ* (December 2000) 387.
9. Da Prat, G.: *Well Test Analysis for Fractured Reservoir Evaluation,* Elsevier Science Publishing Co., New York City (1990).
10. Muskat, M.: *The Flow of Homogeneous Fluids Through Porous Media,* J.W. Edwards Inc., Ann Arbor, Michigan (1946).
11. Shashkov, M.: *Conservative Finite-Difference Methods on General Grids,* CRC Press, Boca Raton, Florida (1995).
12. Shashkov, M. and Steinberg, S.: "Solving Diffusion Equations With Rough Coefficients in Rough Grids," *J. Comp. Phys.* (1996) **129,** 383.
13. Carslaw, J.C. and Jaeger, J.C.: *Conduction of Heat in Solids,* Clarendon Press, Oxford, U.K. (1959).
14. Tikhonov, A.N. and Samarskii, A.A.: *Equations of Mathematical Physics,* International Series of Monographs in Pure and Applied Mathematics, Macmillan Publishing Co., New York City (1963) v. 39.
15. Narasimhan, T.N. and Witherspoon, P.A.: "An Integrated Finite Difference Method for Analyzing Fluid Flow in Porous Media," *Water Resour. Res.* (1976) **12,** No. 1, 57.
16. Bertsekas, D.P.: *Constrained Optimization and Lagrange Multiplier Methods,* Academic Press, New York City (1982).
17. Hildebrand, F.B.: *Introduction to Numerical Analysis,* McGraw-Hill, New York City (1956).
18. Vasil'ev, F.P.: *Numerical Methods for Solving Extremal Problems* (in Russian), Nauka Publishers, Moscow (1982).
19. Jegou, S.: "Using Maple for Symbolic Differentiation to Solve Inverse Problems," *Maple Tech.* (1997) **4,** 32.

Appendix A—Discretization of Gauss-Ostrogradski Divergence Theorem

Here we outline the main aspects of the method of support operators we use to identify the anisotropy of permeability tensor. The theory of the method is explained in more detail in Ref. 11.

First, let us recall the Gauss-Ostrogradski divergence theorem: given a vector field w and a scalar function p (in our case p is the pressure) defined over a domain Ω with the boundary $\Gamma = \partial\Omega$, the following equality holds true:

$$\int_{\Omega} p\nabla \cdot w d\Omega + \int_{\Omega} \nabla p \cdot w d\Omega = \int_{\Gamma} pw \cdot n d\Gamma, \quad \text{.....(A-1)}$$

where n is the outer normal at the surface Γ. We assume that both the vector field w and function p are smooth enough and that the domain Ω has sufficiently regular boundary. Here we need a slight modification of Eq. A-1. If $\vec{k}$ is a symmetric positive definite tensor defined on $\Omega \cup \Gamma$, then

$$\int_{\Omega} \vec{k}\nabla p \cdot \vec{k}^{-1} w d\Omega = \int_{\Gamma} pw \cdot n d\Gamma - \int_{\Omega} p\nabla \cdot w d\Omega. \quad \text{.....(A-2)}$$

Eq. A-2 can be interpreted as the definition of the flux operator $\vec{k}\nabla p$. Indeed, if we pick a smooth function p defined over $\Omega \cup \Gamma$, then there exists only one vector field u such that

$$\int_{\Omega} u \cdot \vec{k}^{-1} w d\Omega = \int_{\Gamma} pw \cdot n d\Gamma - \int_{\Omega} p\nabla \cdot w d\Omega \quad \text{.....(A-3)}$$

holds true for an arbitrary vector field w. From Eq. A-2, $u = \vec{k}\nabla p$. Therefore, the definition of the flux operator is given through the divergence operator. In a sense, the flux operator is "supported" by the divergence and vice versa. This property is the foundation of the method of support operators.

Theoretically, Eq. A-3 can be "reversed." The divergence can be defined through the flux operator (i.e., the divergence and flux are dual to each other). Practically, it is more natural to use Eqs. A-2 and A-3 to define flux through divergence, rather than vice versa.

In order to use the definition in Eq. A-3 for discretizing Eq. 1, we need to take the following steps. First, we discretize the divergence. Then, using this discretization, we discretize Eq. A-3. The third step is to resolve Eq. A-3 with respect to u. Because the right-hand side is linear with respect to p, we will treat u as a linear transformation of p, which reduces to a matrix in the discretized equation. After all these steps are accomplished, it only remains to superimpose the discretized divergence and flux in order to obtain a discretization of the boundary-value problem presented in Eqs. 1 and 2.

Discretization of Divergence. By definition, the divergence of the vector field w is equal to

$$\nabla \cdot w = \lim_{|V| \to 0} \frac{1}{|V|} \int_{\partial V} w \cdot n ds. \quad \text{.....(A-4)}$$

Here, $|V|$ denotes the volume of domain V, which contracts to a point as we pass to the limit; n is the outer unit normal to V at its boundary ∂V at a surface element ds. If we replace the limit in Eq. A-4 by the same expression evaluated on a finite domain V, we obtain a discrete approximation of divergence. It is not difficult to show that this approximation is of second order with respect to the size of domain V, if divergence is evaluated at the centroid of V and the surface integral is evaluated exactly.

Consider a 2D grid Ω_h with quadrilateral cells. Consider a cell (i, j), $1 \le i \le N_x$, $1 \le j \le N_y$. Given a vector field w, denote by $f_{ij}^{1,2,3,4}$ its normal components at the four boundaries of the cell (i, j). We assume the positive directions to be north and east [i.e., $f_{ij}^{1,4}$ are normal fluxes from outside into cell (i, j), whereas $f_{ij}^{2,3}$ are fluxes from cell (i, j) to outside (see Fig. 2)]. Note that each f_{ij}^{m}, $m = 1,2,3,4,$ is a scalar. Therefore, by taking a cell as a finite small domain for the computation of the approximate divergence, we obtain

$$\left([\mathbf{D}]f\right)_{ij} = \frac{1}{A_{ij}} \sum_{m=1}^{4} f_{ij}^{m} l_{ij}^{m}, \quad \text{.....(A-5)}$$

where $l_{ij}^{1,2,3,4}$ are the areas (here lengths) of the side faces of the cell (i,j), and A_{ij} is the volume (here area) of cell (i,j). As in Ref. 11, we formally extend $[\mathbf{D}]$ to the boundary of Ω_h by putting $\left([\mathbf{D}]f\right)_{ij} = -f_{ij}^{m}$, where m is the index of the cell edge along the boundary of Ω_h **(Fig. 9).** In the case of the Dirichlet boundary condition, this extension is not important and it is done here only for consistency.

The normal component of the flux is continuous across the boundary of the cell even for heterogeneous and anisotropic media. The vector field w is evaluated at the vertices of the cell, and we denote its corresponding values by $W_{ij}^{1,2,3,4}$ (Fig. 2). Clearly, the projections of vectors $W_{ij}^{1,2,3,4}$ on the respective outer unit normals $n_{ij}^{1,2,3,4}$, yield $f_{ij}^{1,2,3,4}$ with appropriate signs. Therefore, there is a linear transformation mapping the array W of all flux vectors $W_{ij}^{1,2,3,4}$ evaluated in every vertex of the grid cell to the array f of all $f_{ij}^{1,2,3,4}$. This transformation can be obtained through quite cumbersome but straightforward calculations. Moreover, it can be verified that there also exists an inverse transformation of the array f into an array W, and this inverse transformation can be explicitly calculated as well. Let us denote the transformation mapping f into W by $[\mathbf{\Phi}]$

$$W = [\mathbf{\Phi}]f. \quad \text{.....(A-6)}$$

The structure of matrix $[\mathbf{\Phi}]$ is determined by the structure of grid

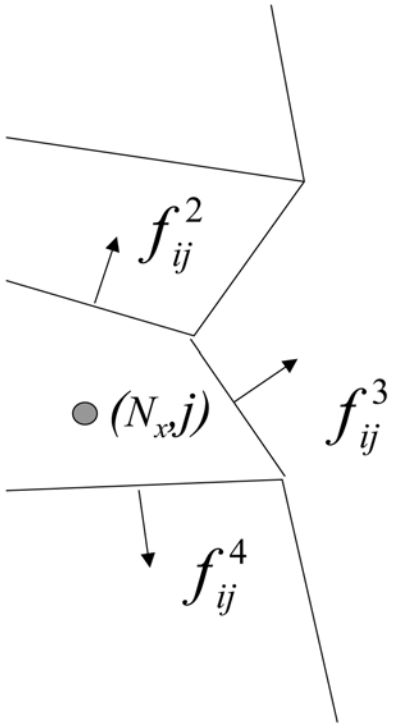

Fig. 9—Formal extension of $[\mathbf{D}]$ to the boundary:

Ω_h only, and there is no dependence on *W* or *f*. Summing up, the discretization of divergence given by Eq. A-5 can be equivalently formulated in terms of discretization of vector field w

$$[\mathbf{D}]f = [\mathbf{D}][\mathbf{\Phi}]^{-1} W. \quad \text{.....(A-7)}$$

Discretization of the Integrals in Eq. A-2. Eq. A-2 involves two kinds of integrals: two integrals over domain Ω, and one surface integral over $\Gamma = \partial\Omega$. In our case, the boundary of the discretized domain, Ω_h, is given by a closed polygonal line; for the surface integral we apply the quadrature rule of rectangles with the integrand evaluated at the midpoint[17]:

$$\int_\Gamma pw \cdot nd\Gamma = \sum_{j=1}^{N_y} \left(P_{1/2\ j} f^1_{1j} l^1_{1j} + P_{N_x+1/2\ j} f^3_{N_x\ j} l^3_{N_x\ j} \right) + \sum_{i=1}^{N_x} \left(P_{i\ 1/2} f^4_{i1} l^4_{i1} + P_{i\ N_y+1/2} f^2_{i\ N_y} l^2_{i\ N_y} \right) \quad \text{. (A-8)}$$

The integral $\int_\Omega p\nabla \cdot wd\Omega$ can be discretized straightforwardly, because the integrand is evaluated at the centroid of each cell:

$$\int_\Omega p\nabla \cdot wd\Omega \approx \sum_{i=1}^{N_x} \sum_{j=1}^{N_y} u_{ij} \left([\mathbf{D}]f \right)_{ij} A_{ij} = [\mathbf{\Lambda}]u \cdot [\mathbf{D}]f, \quad \text{(A-9)}$$

where $[\mathbf{\Lambda}]$ = a diagonal matrix whose elements are equal to A_{ij}. In particular, matrix $[\mathbf{\Lambda}]$ is positive definite. The dot-product on the right side of Eq. A-9 is equal to the sum of products of individual components over to all indices *i*, *j*.

Substitution of Eq. A-5 into Eq. A-9 yields

$$\int_\Omega p\nabla \cdot wd\Omega \approx \sum_{i=1}^{N_x} \sum_{j=1}^{N_y} P_{ij} \sum_{m=1}^{4} f^m_{ij} l^m_{ij}, \quad \text{.....(A-10)}$$

where coefficients l^m_{ij} are defined above, see Eq. A-5.

Now let us discretize the integral on the left side of Eq. A-3:

$$I = \int_\Omega u \cdot \vec{\vec{k}}^{-1} wd\Omega. \quad \text{.....(A-11)}$$

$$[\mathbf{D}]f = [\mathbf{D}][\mathbf{\Phi}]^{-1} W. \quad \text{.....(A-12)}$$

Discretization of the Integrals in Eq. A-2. Eq. A-2 involves two kinds of integrals: two integrals over domain Ω, and one surface integral over $\Gamma = \partial\Omega$. In our case, the boundary of the discretized domain, Ω_h, is given by a closed polygonal line; for the surface integral we apply the quadrature rule of rectangles with the integrand evaluated at the midpoint[17]:

$$\int_\Gamma pw \cdot nd\Gamma = \sum_{j=1}^{N_y} \left(P_{1/2\ j} f^1_{1j} l^1_{1j} + P_{N_x+1/2\ j} f^3_{N_x\ j} l^3_{N_x\ j} \right) + \sum_{i=1}^{N_x} \left(P_{i\ 1/2} f^4_{i1} l^4_{i1} + P_{i\ N_y+1/2} f^2_{i\ N_y} l^2_{i\ N_y} \right) \quad \text{.... (A-13)}$$

The integral $\int_\Omega p\nabla \cdot wd\Omega$ can be discretized straightforwardly, because the integrand is evaluated at the centroid of each cell:

$$\int_\Omega p\nabla \cdot wd\Omega \approx \sum_{i=1}^{N_x} \sum_{j=1}^{N_y} u_{ij} \left([\mathbf{D}]f \right)_{ij} A_{ij} = [\mathbf{\Lambda}]u \cdot [\mathbf{D}]f, \text{(A-14)}$$

where $[\mathbf{\Lambda}]$ = a diagonal matrix whose elements are equal to A_{ij}. In particular, matrix $[\mathbf{\Lambda}]$ is positive definite. The dot-product on the right side of Eq. A-9 is equal to the sum of products of individual components over to all indices *i*, *j*.

Substitution of Eq. A-5 into Eq. A-9 yields

$$\int_\Omega p\nabla \cdot wd\Omega \approx \sum_{i=1}^{N_x} \sum_{j=1}^{N_y} P_{ij} \sum_{m=1}^{4} f^m_{ij} l^m_{ij}, \quad \text{.....(A-15)}$$

where coefficients l^m_{ij} are defined above, see Eq. A-5.

Now let us discretize the integral on the left side of Eq. A-3:

$$I = \int_\Omega u \cdot \vec{\vec{k}}^{-1} wd\Omega. \quad \text{.....(A-16)}$$

Because the discretized vector fields are evaluated at the corners of the grid cells, the numerical integration of the scalar product in Eq. A-11 reduces to the problem of numerical integration of a scalar function $z = u \cdot \vec{\vec{k}}^{-1} w$ evaluated at the vertices of the cells. At each vertex, however, the function may take up to four different values affiliated with neighboring cells for which the vertex is common. Consequently, we calculate the integral over each individual cell and then sum up over all cells.

Denote the values of the scalar product *z* affiliated with cell (*i*, *j*) by $Z^{1,2,3,4}_{ij}$:

$$Z^m_{ij} = U^m_{ij} \cdot \vec{\vec{k}}^{-1} W^m_{ij} \quad m = 1,2,3,4, \quad \text{.....(A-17)}$$

where U^m_{ij} and W^m_{ij} are the vector fields *u* and *w* evaluated at *m*-th vertex of cell (*i*, *j*) **(Fig. 10).** Denote by $\beta^{1,2,3,4}_{ij}$ the cubature coefficients for the numerical integration over cell (*i*,*j*). The integral of the discrete function *z* over the cell is then given by

$$I_{ij} = \sum_{m=1}^{4} \beta^m_{ij} Z^m_{ij}. \quad \text{.....(A-18)}$$

There are several different ways to define the coefficients $\beta^{1,2,3,4}_{ij}$. In the examples below, $\beta^{1,2,3,4}_{ij}$ were defined in such a way that Eq. A-13 provided exact evaluation of integrals of a constant, of a linear function and of the product *xy*. Therefore, at each cell the coefficients $\beta^{1,2,3,4}_{ij}$ are found from solution to a system of four linear equations. Clearly, cubature coefficients $\beta^{1,2,3,4}_{ij}$ depend only on the structure of the grid but not on the vector fields *u* and *w*.

Summing up over all indices *i, j*, we obtain

$$I \approx \sum_{i=1}^{N_x}\sum_{j=1}^{N_y}\sum_{m=1}^{4} \beta_{ij}^{m} U_{ij}^{m} \cdot \vec{k}^{-1} W_{ij}^{m}. \quad \text{.....(A-19)}$$

It is possible to prove that if the cubature coefficients $\beta_{ij}^{1,2,3,4}$ are selected as described above, then the accuracy of approximation of integral on the left side of Eq. A-3 by Eq. A-14 is of second order with respect to the largest diameter of the cells. The iterated sum on the right side of Eq. A-14 is a bilinear form with respect to U and W. Let us write it down in matrix notation:

$$\sum_{i=1}^{N_x}\sum_{j=1}^{N_y}\sum_{m=1}^{4} \beta_{ij}^{m} U_{ij}^{m} \cdot \vec{k}^{-1} W_{ij}^{m} = [\mathbf{B}] U \cdot \left[\mathbf{K^1}\right] W, \quad \text{.....(A-20)}$$

where $[\mathbf{B}]$ is the diagonal matrix of coefficients $\beta_{ij}^{1,2,3,4}$ and $\left[\mathbf{K^1}\right]$ is the matrix derived from the inverse tensor $\vec{k}^{-1}$. Clearly, $\left[\mathbf{K^1}\right]$ is symmetric and positive definite. Let us assume that every cell of grid Ω_h is convex; then all cubature coefficients are nonnegative: $\beta_{ij}^{m} \geq 0$. Interchanging U and V does not affect the sum in Eq. A-15; therefore, matrix $\left[\mathbf{K^1}\right][\mathbf{B}]$ is symmetric and positive definite as well.

Denote by $[\mathbf{F}]$ the matrix discretizing the normal component of flux operator at each cell:

$$\vec{k}\nabla p \cdot n_{ij}^{m} \approx [\mathbf{F}] P, \quad \text{.....(A-21)}$$

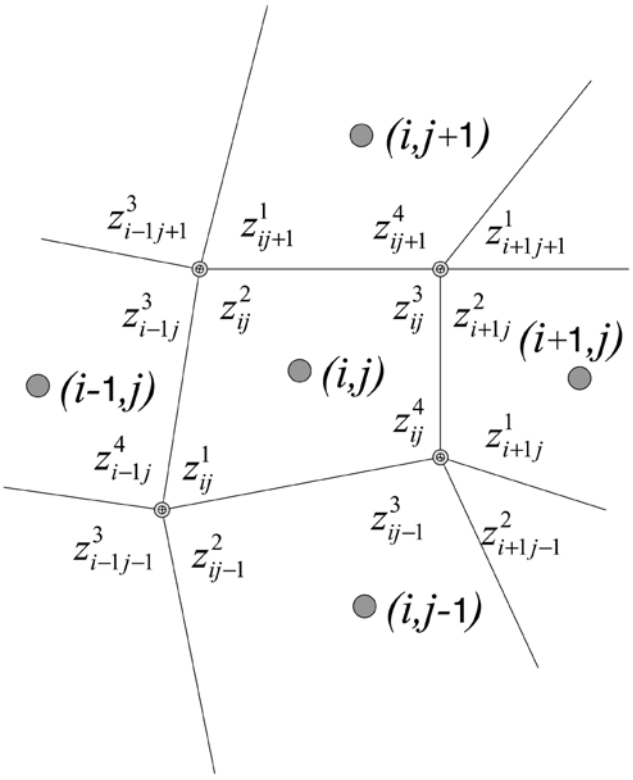

Fig. 10—The scalar function *z* may take up to four different values at each vertex of the cell (*i,j*).

where P = the array of the values of pressure at the centroid of each cell. In other words, on the boundaries of each cell matrix $[\mathbf{F}]$ maps P into an array of normal fluxes. Therefore, combining Eqs. A-6, A-11, and A-14 through A-16, we obtain

$$\int_{\Omega} \vec{k}\nabla p \cdot \vec{k}^{-1} w d\Omega \approx [\mathbf{\Phi}][\mathbf{F}] P \cdot \left[\mathbf{K^1}\right][\mathbf{B}][\mathbf{\Phi}] f \ . \ . \text{(A-22)}$$

Finally, the discretization of the Gauss-Ostrogradski divergence theorem yields the following equation

$$\begin{aligned}[\mathbf{F}] P \cdot [\mathbf{\Phi}]^{*} \left[\mathbf{K^1}\right][\mathbf{B}][\mathbf{\Phi}] f \\ = -[\mathbf{\Lambda}] P \cdot [\mathbf{D}] f \\ \sum_{j=1}^{N_y} \left(P_{1/2\,j} f_{1j}^{1} l_{1j}^{1} + P_{N_x+1/2\,j} f_{N_x\,j}^{3} l_{N_x\,j}^{3} \right) \text{.....(A-18)} \\ + \sum_{i=1}^{N_x} \left(P_{i\,1/2} f_{i1}^{4} l_{i1}^{4} + P_{i\,N_y+1/2} f_{i\,N_y}^{2} l_{i\,N_y}^{2} \right)\end{aligned}$$

As Eq. A-18 holds true for an arbitrary pair of vectors P and f, it actually defines the flux operator matrix $[\mathbf{F}]$. From a practical point of view, it is useful to note that A_{ij} cancels in the first term on the right side of Eq. A-18.

Appendix B—Gradient of Functional (Eq. 11) Adjoint System

Let us derive the adjoint system for the problem of minimization of functional (Eq. 11), subject to the constraint specified by the boundary-value problem in Eqs. 1 and 2. This is a standard method of deriving the gradient in a constrained optimization problem.[18] Assume a small perturbation $\delta\vec{k}$ of the permeability tensor $\vec{k}$ such that $\vec{k} + \delta\vec{k}$ also is a symmetric positive tensor. Then put $J\left[\vec{k}\right] + \delta J = J\left[\vec{k} + \delta\vec{k}\right]$ and denote by $p + \delta p$ the solution to the boundary-value problem

$$\nabla \cdot \left[\left(\vec{k} + \delta\vec{k} \right) \nabla \left(p + \delta p \right) \right] = -q, \ \ (x,y) \in \Omega, \ldots\ldots (1_{\delta})$$

$$\left(p + \delta p \right)\big|_{\Gamma} = p_0 \ldots\ldots\ldots\ldots\ldots\ldots\ldots\ldots\ldots\ldots (2_{\delta})$$

Neglecting the terms of order higher than one, we obtain

$$\delta J = \int_{\Omega} \Xi(x,y) \left[p(x,y) - p_{*}(x,y) \right] \delta p(x,y) d\Omega, \quad \text{.....(B-1)}$$

where δp satisfies the boundary-value problem in variations

$$\nabla \cdot \left(\delta\vec{k} \nabla p \right) + \nabla \cdot \left[\vec{k} \nabla \left(\delta p \right) \right] = 0, \quad \text{.....(B-2)}$$

$$\delta p\big|_{\Gamma} = 0. \quad \text{.....(B-3)}$$

Multiply Eq. B-2 by an adjoint variable $\psi(x,y)$, integrate over Ω and add to Eq. B-1. Then

$$\delta J = \int_{\Omega} \Xi(x,y) \left[p(x,y) - p_{*}(x,y) \right] \delta p(x,y) d\Omega$$

$$+\int_{\Omega}\psi\nabla\cdot\left(\delta\vec{\vec{k}}\nabla p\right)+\psi\nabla\cdot\left[\vec{\vec{k}}\nabla(\delta p)\right]d\Omega \quad \text{.....(B-4)}$$

Using the Gauss-Ostrogradski divergence theorem and taking into account Eq. B-3, we obtain

$$\int_{\Omega}\psi\nabla\cdot\left(\delta\vec{\vec{k}}\nabla p\right)+\psi\nabla\cdot\left(\vec{\vec{k}}\nabla(\delta p)\right)d\Omega$$
$$=\int_{\Omega}-\nabla\psi\cdot\left(\delta\vec{\vec{k}}\nabla p\right)+\delta p\nabla\cdot\left(\vec{\vec{k}}\nabla\psi\right)d\Omega \quad \text{.....(B-5)}$$
$$\int\psi\left(\delta\vec{\vec{k}}\nabla p+\vec{\vec{k}}\delta p\right)nd\Gamma.$$

Now, if $\psi(x,y)$ solves the adjoint boundary-value problem

$$\nabla\cdot\left(\vec{\vec{k}}\nabla\psi\right)=-\Xi(p-p_*) \quad \text{.....(B-6)}$$

$$\psi\big|_{\Gamma}=0 \quad \text{.....(B-7)}$$

then, from Eqs. B-4 and B-5, the variation of the functional in Eq. 11 is equal to

$$\delta J=-\int_{\Omega}\nabla\psi\cdot\left(\delta\vec{\vec{k}}\nabla p\right)d\Omega. \quad \text{.....(B-8)}$$

Appendix C—Differential of Second Order by Second Adjoint System

The analysis presented in Appendix B can be extended to the calculation of the second differential of functional (Eq. 11). In this appendix, we derive the second adjoint system of equations and express the second order derivative of Eq. 11 through the solution of the second adjoint system. In a general case, the second-order differential is a quadratic form over a functional space,[18] and the calculations can be rather complicated. It is easier to calculate a directional derivative, rather than the Hessian. However, in our particular situation there is only one optimization parameter. Consequently, the calculations can be completed, and we derive a pair of coupled boundary-value problems of the same type as Eqs. 1 and 2.

Because the second derivative is the derivative of the first derivative, we can calculate $\frac{d^2}{d\theta^2}J(\theta)$ in a similar way as we obtained Eq. 18. Indeed, in order to calculate Eq. 18, we solve a pair of boundary-value problems (Eqs. 1 and 2 and B-6 and B-7). Therefore, we can interpret Eq. 18 as another functional and Eqs. 1, 2, B-6, and B-7 as a system of constraints. Then, assuming a small variation $\delta\theta$ of θ, we obtain

$$\delta g(\theta)=-\int_{\Omega}\nabla\delta\psi\cdot\left(\frac{d}{d\theta}\vec{\vec{k}}(\theta)\nabla p\right)d\Omega$$
$$-\int_{\Omega}\nabla\delta\psi\cdot\left(\frac{d^2}{d\theta^2}\vec{\vec{k}}(\theta)\nabla p\right)d\Omega\delta\theta \quad \text{.....(C-4)}$$
$$-\int_{\Omega}\nabla\delta\psi\cdot\left(\frac{d}{d\theta}\vec{\vec{k}}(\theta)\nabla(\delta p)\right)d\Omega\delta\theta,$$

where $g(\theta)=\frac{dJ(\theta)}{d\theta}$. Similar to Eqs. B-2 and B-3 in Appendix B, we obtain the following tangent boundary-value problems for variations δp and $\delta\psi$:

$$\nabla\cdot\left[\frac{d}{d\theta}\vec{\vec{k}}(\theta)\nabla p\right]\delta\theta$$
$$+\nabla\cdot\left[\vec{\vec{k}}(\theta)\nabla(\delta p)\right]=0\,(x,y)\in\Omega \quad \text{, ...(C-2)}$$

$$\delta p\big|_{\Gamma}=0, \quad \text{.....(C-3)}$$

and

$$\nabla\cdot\left[\frac{d}{d\theta}\vec{\vec{k}}(\theta)\nabla\psi\right]\delta\theta+\nabla\cdot\left[\vec{\vec{k}}(\theta)\nabla(\delta\psi)\right]$$
$$+\Xi\delta p=0\,(x,y)\in\Omega \quad \text{, ...(C-4)}$$

$$\delta\psi\big|_{\Gamma}=0. \quad \text{.....(C-5)}$$

Now let us introduce two auxiliary adjoint variables, $\psi_1(x,y)$ and $\psi_2(x,y)$. Multiply Eqs. C-2 and C-4 by $\psi_1(x,y)$ and $\psi_2(x,y)$, respectively; integrate the result over Ω and add to Eq. C-1. Straightforward calculations involving several iterations of the Gauss-Ostrogradski divergence theorem yield

$$\delta g(\theta)=-\int_{\Omega}\nabla\psi\cdot\left[\frac{d^2}{d\theta^2}\vec{\vec{k}}(\theta)\nabla p\right]d\Omega\delta\theta$$
$$-\int_{\Omega}\nabla\psi_1\cdot\left[\frac{d}{d\theta}\vec{\vec{k}}(\theta)\nabla p\right]d\Omega\delta\theta$$
$$-\int_{\Omega}\nabla\psi_2\cdot\left[\frac{d}{d\theta}\vec{\vec{k}}(\theta)\nabla\psi\right]d\Omega\delta\theta$$
$$+\int_{\Omega}\left\{\nabla\cdot\vec{\vec{k}}(\theta)\nabla\psi_2-\nabla\cdot\left[\frac{d}{d\theta}\vec{\vec{k}}(\theta)\nabla p\right]\right\}\delta d\Omega$$
$$+\int_{\Omega}\left\{\nabla\cdot\vec{\vec{k}}(\theta)\nabla\psi_1-\nabla\cdot\left[\frac{d}{d\theta}\vec{\vec{k}}(\theta)\nabla\psi\right]+\Xi\psi_2\right\}\delta p d\Omega$$
$$+\int_{\Gamma}\psi_1\nabla\cdot\left[\vec{\vec{k}}(\theta)\nabla\delta p\right]d\Gamma$$
$$+\int_{\Gamma}\psi_2\nabla\cdot\left[\vec{\vec{k}}(\theta)\nabla\delta\psi\right]d\Gamma. \quad \text{.....(C-6)}$$

Finally, we obtain that

$$\frac{d^2J}{d\theta^2}=-\int_{\Omega}\nabla\psi\cdot\left[\frac{d^2}{d\theta^2}\vec{\vec{k}}(\theta)\nabla p\right]d\Omega$$
$$+\int_{\Omega}\nabla\psi_1\cdot\left[\frac{d}{d\theta}\vec{\vec{k}}(\theta)\nabla p\right]d\Omega \quad \text{, ...(C-7)}$$
$$+\int_{\Omega}\nabla\psi_2\cdot\left[\frac{d}{d\theta}\vec{\vec{k}}(\theta)\nabla\psi\right]d\Omega$$

where p = the solution to the forward problem (Eqs. 1 and 2), ψ = the solution to the first adjoint problem (Eqs. B-2 and B-3), and ψ_1, ψ_2 are, respectively, the solutions to the following pair of boundary value problems:

$$\nabla\cdot\left[\vec{\vec{k}}(\theta)\nabla\psi_1\right]=\nabla\cdot\left[\frac{d}{d\theta}\vec{\vec{k}}(\theta)\nabla\psi\right]-\Xi\psi_2, \quad \text{.....(C-8)}$$

$$\psi_1\big|_\Gamma = 0\,, \quad \text{.....(C-9)}$$

$$\nabla\cdot\left[\vec{\vec{k}}(\theta)\nabla\psi_2\right] = \nabla\cdot\left[\frac{d}{d\theta}\vec{\vec{k}}(\theta)\nabla p\right], \quad \text{.....(C-10)}$$

$$\psi_2\big|_\Gamma = 0\,. \quad \text{.....(C-11)}$$

which yield the second adjoint system. Note that Eqs. 1, C-4, C-8, and C-10 are replicas of the same elliptic equation with different right sides. The same holds true with regard to the boundary conditions. Therefore, the same discretization and solution routines can be used for all of them.

Summing up, in order to find the second derivative of functional (Eq. 11), first, we solve the forward problem (Eqs. 1 and 2); second, we solve the first adjoint problem (Eqs. B-2 and B-3); and third, we solve the boundary problems (Eqs. C-8 and C-11).

Second-order derivatives are used in Newton's descent method, which is very efficient in minimization. In many cases, given a good initial guess, Newton's method provides convergence to the solution in a few iterations.[18] However, there is an overhead of solving four boundary-value problems per iteration. Moreover, as the number of optimization parameters increases, the number of boundary-value problems solved to calculate the second differential of the functional increases as well.

Appendix D—Discrete Version of Adjoint System and the Gradient

In Appendix B, we have derived the adjoint system for calculating the gradient of the functional in Eq. 11, subject to constraints (Eqs. 1 and 2). In effect, the forward and adjoint problems have been discretized independently of each other. This circumstance does not cause any problems in our particular case, because our discretization produces a symmetric positive definite matrix. In a general case, however, the discretization of the adjoint problem depends on the discretization of the forward problem. Both discretizations will be appropriately coupled if we first discretize the forward problem and then derive the adjoint system in discretized form. The latter approach usually leads to cumbersome calculations, because the discrete system of equations has multiple indices. A software package admitting symbolic computations could be useful to avoid errors (Ref. 19).

The support-operators method allows us to reduce the burden of calculations because of the clear matrix representation (Eqs. 8 and 10) of the discrete equations. In this appendix, we obtain the system of equations adjoint to Eq. 8.

Note that in Eqs. 8 and 10, only matrix $[\mathbf{K}]$ depends on the optimization parameter θ. Therefore, if θ is perturbed by a small variation $\delta\theta$, then the equation in variations is

$$\delta[\mathbf{A}]P + [\mathbf{A}]\delta P = \delta B\,. \quad \text{.....(D-1)}$$

The variation of the functional in Eq. 20 is equal to

$$\delta J = \sum_{i=1}^{N_x}\sum_{j=1}^{N_y}\Xi_{ij}\left(P_{ij} - P_{*ij}\right)A_{ij}\delta P_{ij}\,. \quad \text{.....(D-2)}$$

Let us introduce the adjoint discrete variable ψ_{ij}. Multiply Eq. D-1 by $\Psi_{ij}A_{ij}$ element by element and add the sum over all *i, j* to Eq. D-2. We obtain

$$\delta J = \sum_{i=1}^{N_x}\sum_{j=1}^{N_y}\left[\Xi_{ij}\left(P_{ij} - P_{*ij}\right) + \left([\mathbf{A}]\Psi\right)_{ij}\right]A_{ij}\delta P_{ij} + \sum_{i=1}^{N_x}\sum_{j=1}^{N_y}\left[\left(\delta[A]\Psi\right)_{ij} - \delta B_{ij}\Psi_{ij}\right]A_{ij}\,. \quad \text{.....(D-3)}$$

Because of Eqs. 9 and 10, to calculate $\delta[\mathbf{A}]$ and δB we also need to calculate the variation of matrix $\left([\Phi]^*[\mathbf{K}^1][\mathbf{B}][\Phi]\right)^{-1}$. Calculations yield:

$$\begin{aligned}&\delta\left([\Phi]^*[\mathbf{K}^1][\mathbf{B}][\Phi]\right)^{-1}\\ &= \left([\Phi]^*[\mathbf{K}^1][\mathbf{B}][\Phi]\right)^{-1}\\ &\times[\Phi]^*\left(\frac{d}{d\theta}[\mathbf{K}^1]\right)\\ &\times[\mathbf{B}][\Phi]\left([\Phi]^*[\mathbf{K}^1][\mathbf{B}][\Phi]\right)^{-1}\delta\theta\end{aligned} \quad \text{.....(D-4)}$$

Further, $[\mathbf{K}^1]$ depends linearly on $\vec{\vec{k}}(\theta)^{-1}$ (see Eq. A-15). Therefore,

$$\frac{d}{d\theta}\left\{K^1\left[\vec{\vec{k}}(\theta)^{-1}\right]\right\} = \left\{K^1\left[\frac{d}{d\theta}\vec{\vec{k}}(\theta)^{-1}\right]\right\}, \quad \text{.....(D-5)}$$

where

$$\frac{d}{d\theta}\vec{\vec{k}}(\theta)^{-1} = \vec{\vec{k}}(\theta)^{-1}\left[\frac{d}{d\theta}\vec{\vec{k}}(\theta)\right]\vec{\vec{k}}(\theta)^{-1}, \quad \text{.....(D-6)}$$

and for $\frac{d}{d\theta}\vec{\vec{k}}(\theta)$ we already have formula (Eq. 17).

Thus, from Eqs. D-2 through D-4, we finally obtain

$$\begin{aligned}\frac{dJ}{d\theta} = \sum_{i=1}^{N_x}\sum_{j=1}^{N_y}\Bigg\{&\Bigg[\Bigg(\Big([\Lambda][\mathbf{D}]\left([\Phi]^*[\mathbf{K}^1][\mathbf{B}][\Phi]\right)^{-1}\\ &\times\frac{d}{d\theta}[\mathbf{K}^1][\mathbf{B}][\Phi][\mathbf{F}]\Big)^*\Psi\Bigg]_{ij}\\ &+\Bigg[\left([\Phi]^*[\mathbf{K}^1][\mathbf{B}][\Phi]\right)^{-1}\frac{d}{d\theta}[\mathbf{K}^1][\mathbf{B}][\Phi]\\ &\times\left([\Phi]^*[\mathbf{K}^1][\mathbf{B}][\Phi]\right)^{-1}[\Lambda_b]P_b\Bigg]_{ij}\Psi_{ij}\Bigg\}A_{ij}\end{aligned} \quad \text{, .(D-7)}$$

where $\frac{d}{d\theta}[\mathbf{K}^1]$ is calculated through Eqs. D-5 and D-6.

Dmitriy B. Silin is a geological scientist at the Earth Sciences Div. of Ernest Orlando Lawrence Berkeley Natl. Laboratory. e-mail: Dsilin@lbl.gov. For five years he was an associate professor at M.V. Lomonosov Moscow State U. He holds MS and PhD degrees in applied mathematics from the Dept. of Computational Mathematics and Cybernetics at M.V. Lomonosov Moscow State U. Silin also obtained the degree of Doctor of Physical and Mathematical Sciences in 1993. **Tad W. Patzek** is professor of GeoEngineering at the Dept. of Civil and Environmental Engineering, U. of California, Berkeley. e-mail: patzek@patzek.berkeley.edu. Prior to joining Berkeley, he was a senior reservoir engineer at Shell Western E&P Inc. (1989–90); senior research engineer (1986–89) and research engineer (1983–86) at the Enhanced Recovery Research Dept., Shell Development; research associate at the Chemical Engineering Dept., U. of Minnesota (1981–83); and research associate at Chemical Engineering Research Center, Polish Academy of Sciences, Gliwice, Poland. Patzek has authored 90 papers, 38 industrial reports, and 15 expert witness reports and depositions. In 1995, Patzek was a Distinguished Lecturer for SPE, and he is a member of the SPE Speakers Bureau.